International Forum on Aeroelasticity and Structural Dynamics
IFASD 2022
13-17 June 2022, Madrid, Spain

GUST LOAD ALLEVIATION CONTROL RELATED METRIC FOR MULTIDISCIPLINARY DESIGN OPTIMIZATION

Bernardo Bahia Monteiro[1], Carlos E. S. Cesnik[1], Ilya Kolmanovsky[1], Fabio Vetrano[2]

[1]Department of Aerospace Engineering, University of Michigan
Francois-Xavier Bagnoud Building, 1320 Beal Ave, Ann Arbor, MI 48109
{bbahia, cesnik, ilya}@umich.edu

[2]Airbus Operations S.A.S.
fabio.vetrano@airbus.com

Keywords: Gust load alleviation, multidisciplinary design optimization, feedback control, Bode integral relation

Abstract:

This paper presents a new approach for considering gust load alleviation (GLA) in the multidisciplinary design optimization (MDO) process. Closed-loop control considerations are incorporated into the MDO problem through the inclusion of the parameterization of the aircraft's sensitivity function to stress. The parameters of such function are included as design variables and a constraint on its Bode integral relation is imposed. This approach is control agnostic in the sense that it does not explicitly design the controller or its gains, which can be relegated to a later design phase. It consists in the addition of two constraints to the MDO problem: one for peak gust stress, based on the design envelope criterion, and the other for fatigue life. While the GLA feedback controller does not need to be designed, the optimizer designs the closed-loop sensitivity function directly. An additional constraint on the Bode integral relation is used to ensure that the bandwidth of the system is bounded by the current technological limit, while the parameterization of the sensitivity function is chosen to guarantee robustness of the closed-loop system. Finally, the use of this new approach is be demonstrated by performing multidisciplinary design optimization of a flexible free-flying aircraft model subjected to gust loads.

1 INTRODUCTION

The first time gust load alleviation (GLA) control was considered for multidisciplinary design optimization (MDO) of aircraft was in 1993 [1]. In this study, the structural design of a cantilevered wing was considered simultaneously with the design of a proportional integral (PI) controller that uses the measurement of the wing tip acceleration to command a control surface also located at the tip of the wing. The assumed gust model was stochastic but simplified (based on a first order filter driven by Gaussian white noise), and the analysis was done in time domain.

Renewed interest for MDO in the last decade or so caused the appearance of more studies in this area. Hunten *et al.* [2] showed results of the optimization of a blended wing-body (BWB) configuration using flap deflection for drag reduction, maneuver load alleviation and gust load alleviation, considering only quasi-static gusts and maneuvers. Haghighat *et al.* [3] performed MDO of an aircraft considering a linear quadratic (LQ) controller for reducing gust loads, which

are evaluated in time domain for a $1 - \cos$ type gust. Xu and Kroo [4] performed an aerostructural design optimization of an aircraft considering a proportional derivative control system for GLA, which took the angle of attack as input, and deflections as output for the two most outboard control surfaces on the wing being designed. The gust considered was of the $1 - \cos$ type and the simulation to obtain the gust loads was performed in the time domain.

Most recently, Stanford [5] considered the design of a wingbox with trailing edge control surfaces with GLA, co-designed with a static output feedback controller and control surface sizing. To evaluate the gust loads, the turbulence model was added to the state-space representation of the airplane. No time-domain simulation is performed, instead a Lyapunov equation was solved to obtain the statistics of the stresses due to gust, which are used to inform constraints for the optimization problem.

Meanwhile, work has been done in the design of GLA controllers for fixed plants and few examples are included here to illustrate the type of controller used. Vartio *et al.* [6] designed a linear quadratic Gaussian (LQG) for a half BWB scaled model with multiple trailing edge control surfaces, which was then tested at in free pitch and plunge at the NASA Langley's Transonic Dynamics Tunnel. The closed-loop system exhibited over 50% reduction in gust loads compared to a non-GLA controller. Zeng *et al.* [7] presented an adaptive feedforward controller capable of significantly reducing gust loads in the 2 to 20-Hz range. Dillsaver *et al.* [8] designed LQG controller considering a reduced-order flexible aircraft model and obtained expressive reduction of wing root curvature in simulation. Haghighat *et al.* [9] employed a model predictive controller (MPC) for the GLA problem, and compared its performance with a LQG controller in simulation. Ting *et al.* [10] designed and performed wind tunnel tests of preview H_2 and H_∞ controllers, reporting reduction in the wing root strains for both controllers.

As it can be seen, there is a gap between the techniques employed to design the controllers for a fixed aircraft *versus* the ones used for aircraft control co-design. Moreover, there is no clear choice of control architecture that should be used for GLA. This makes it desirable to develop an approach that guarantees the existence of a controller that gives satisfactory GLA performance for a closed-loop aircraft system without directly designing such controller. This is what it called a controller-agnostic approach. This paper presents one such approach, consisting in the direct optimization of the closed-loop sensitivity transfer function that embodies the combined effects of the aircraft response to control inputs and the feedback controller. This approach avoids restricting the controller architecture from the beginning of the design process and leaves it for later, while guaranteeing desirable closed-loop shaping to the designed sensitivity function [11]. The ultimate goal with this new approach is to ensure that an upper bound on the closed-loop performance informed by the airframe design exists and satisfies the design requirements, thus guaranteeing that a suitable controller exists.

The new approach starts with separating the aircraft plant into a gust response part and a control response part, as shown in Figure 1. The feedback loop consisting of the controller and control response parts of the plant is then considered and characterized by its sensitivity function. This function represents the closed-loop response to a disturbance applied at the plant's output, in this case the gust load. By parameterizing this sensitivity function and using the parameters as additional design variables in the MDO problem, which incorporates a gust load constraint, it is possible to assess the impact of the GLA system on the airframe optimal design. Furthermore, the sensitivity function must satisfy the Bode integral relation, which is incorporated to the problem as an additional constraint. Finally, the peak of the sensitivity function can be bounded

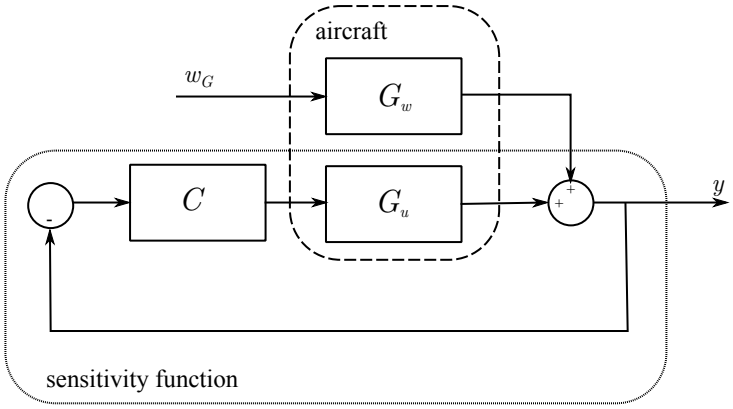

Figure 1: Block diagram of the aircraft closed-loop system partition with a GLA controller.

through the parameterization, which in turn provides bounds to the gain and phase margins [12, 13].

The calculation of gust stresses due to continuous turbulence is done in the frequency domain [14] and is synergistic with the classical control framework (*i.e.*, transfer functions). This procedure allows for very fast evaluation of the gust loads as opposed to time domain simulation, which would have to be run for extended periods of simulated time in order to capture rare gust events.

This paper is organized as follows. Section 2 presents the theoretical framework for the calculation of gust stresses and fatigue damage resulting from a stochastic turbulence input, describes how to incorporate the sensitivity function into that formulation, and formulates the MDO problem that will be solved integrating these elements. Section 3 presents and analyzes the resulting MDO designs, both open and closed-loop solutions. Finally, Section 4 presents the conclusions of this study.

2 THEORETICAL FORMULATION

2.1 Calculation of the stress power spectral distribution due to gust

The procedure to calculate gust loads in the frequency domain described by Hoblit [14] can be extended to evaluate the gust loads of an aircraft equipped with a gust load alleviation system. For that, consider the system shown in Figure 1. In this representation, the aircraft plant is separated into a gust part G_w and a control part G_u, which are then superimposed to generate the aircraft closed-loop stress response σ to a gust disturbance w_G. The closed-loop part of the system is characterized by the sensitivity function,

$$S(s) = \frac{1}{1 + C(s)G_u(s)}, \tag{1}$$

hence the gust-to-load transfer function is $S(s)G_w(s)$, *i.e.*, the closed-loop response is given by the open-loop response filtered by the sensitivity function. The stress power spectral density (PSD) due to gust is thus given by

$$\Phi_\sigma(\omega) = |S(j\omega)|^2 \, |G_w(j\omega)|^2 \, \Phi_{w_G}(\omega), \tag{2}$$

where Φ_σ is the power spectral density of stress due to gust, and Φ_{w_G} is the gust velocity PSD, given by the von Kàrmàn turbulence model as

$$\Phi_{w_G}(\omega) = U_g^2 \frac{L_w}{\pi U_\infty} \frac{1 + \frac{8}{3}(1.339 L_w \omega / U_\infty)^2}{[1 + (1.339 L_w \omega / U_\infty)^2]^{\frac{11}{6}}}, \tag{3}$$

where L_w is the characteristic length of the turbulence, usually of 2500 ft, U_∞ is the flight speed, and U_g is the gust intensity.

The PSD given by Equation (2) is used to obtain the peak gust load and the rate of fatigue damage as discussed in what follows.

2.2 The Bode integral relation

Assuming a linear time invariant (LTI) plant and controller without time delays, the sensitivity function must satisfy the Bode integral relation, which relates the integral of the magnitude of the frequency response of the sensitivity function to the open-loop open right-hand plane (ORHP) poles, *i.e.*,

$$\int_0^\infty \log |S(j\omega)| \mathrm{d}\omega = \pi \sum_{k=1}^{n_u} \mathrm{Re}(\lambda_k) \tag{4}$$

where λ_k, $k = 1, \ldots, n_u$, are the open-loop OHRP poles.

In practice, however, the bandwidth of the controller and actuators is limited, so the Bode integral should be calculated only up to their maximum frequency, instead of over all frequencies [13].

The Bode integral relation is a fundamental control limitation that is able to capture the effects of finite actuation bandwidth and to reflect the inherent difficulty of stabilizing an unstable plant. It ensures that any reduction in sensitivity over some frequency range is accompanied by an increase in sensitivity at other frequencies (the water bed effect), and it reflects the inherent greater dificulty of controlling open-loop unstable designs by yielding an increased integrated value of the sensitivity function in that case. Equation (4) can be used to inform a constraint in MDO.

2.3 Sensitivity function parameterization

In order to design the sensitivity function, it must be parameterized. For this work the sensitivity function is parameterized by considering a series arrangement of a second-order Butterworth high-pass filter and one peaking filter, *i.e.*,

$$S(s) = \underbrace{\frac{s^2 + \omega_c^2}{s^2 + \sqrt{2}\omega_c s + \omega_c^2}}_{\text{high-pass filter}} \underbrace{\frac{s^2 + g_0\omega_0/q_0 + {\omega_0}^2}{s^2 + \omega_0/q_0 + {\omega_0}^2}}_{\text{peaking filter}}. \tag{5}$$

The parameters of the sensitivity function are the high-pass filter's cutoff frequency ω_c, and the peaking filter's gain g_0, center frequency ω_0, and quality factor q_0.

The peak of the magnitude of the sensitivity function is related to the robustness of the closed-loop system, specifically, the sensitivity peak magnitude M_S is the minimum distance between

the Nyquist curve and the critical point -1 [15]. The following bounds on gain and phase margins can be stated in terms of M_S:

$$GM \geq \frac{M_S}{M_S - 1}, \qquad PM \geq 2\sin^{-1}\left(\frac{1}{2M_S}\right). \tag{6}$$

For example, $M_S \leq 2$ guarantees a gain margin of at least 6 dB and phase margin of at least 29°, which are usual requirements for control design.

2.4 Aircraft model and gust-to-stress transfer function

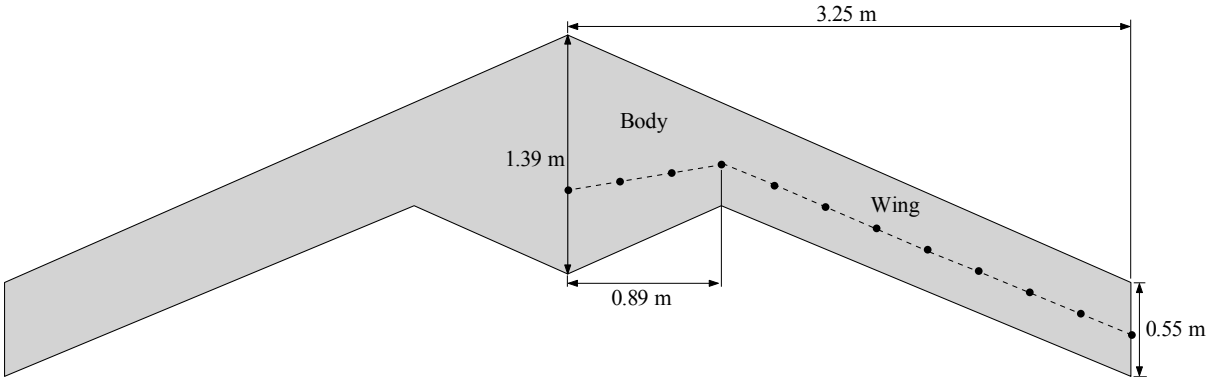

Figure 2: BWB model planform (dashed line: beam reference axis; markers: beam element ends).

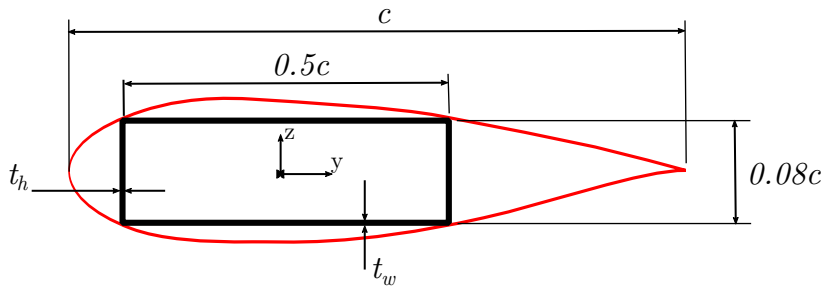

Figure 3: Wingbox cross section for the BWB aircraft.

The aircraft model chosen for this study is a free-flying blended wing-body (BWB) configuration shown in Figure 2, which is simulated using the University of Michigan's Nonlinear Aeroelastic Simulation Toolbox (UM/NAST) [16]. The simple aeroelastic representation is composed of a geometrically exact, strain-based, beam structural model with strip theory aerodynamics. The BWB model consists of three rigid elements with an 80-kg concentrated mass at the nose (the body) and 8 flexible elements with parameterized distributed mass and stiffness (the wing). The aerodynamic coefficients along the span are computed based on the local effective angle of attack using a lookup table for the NACA 0012 airfoil. Three-dimensional effects are approximated by a wingtip loss factor.

The BWB model is linearized using algorithmic differentiation [17] to obtain a state space representation of the dynamic system. It uses an uniform vertical gust speed as input and the curvature at the wing root (element 4 from the left in Figure 2) as the output. Then the transfer function is evaluated based on the state space linearization of the UM/NAST system, that is, if $A_{n\times n}$, $b_{n\times 1}$, $c^T_{n\times 1}$, $d_{1\times 1} = 0$ is the state space representation of the gust-to-stress system, the gust-to-stress transfer function is given by

$$G_w(s) = c^T(sI - A)^{-1}b. \tag{7}$$

In the current formulation, Equation (7) is implemented directly, even though pre-factoring the A matrix can be considered to decrease computational cost [18].

The c^T is chosen to implement the following curvature-to-stress relation at the wing root:

$$\sigma_{\text{gust}} = E\tfrac{h}{2}\,\kappa_{oop}|_{\text{wing root}}. \tag{8}$$

where $\kappa_{oop}|_{\text{wing root}}$ is the out-of-plane curvature evaluated at the wing root

Since this formulation requires a linear transformation from curvature to stress, only the bending stress is considered.

2.5 Calculation of static stress

UM/NAST is built on a condensed model of equivalent beams, so 3D stresses are not directly available from the solution. They must be calculated based on the recovery of the 3D properties from the beam strains considering the knowledge of the material distributions and cross-sectional geometry, shown in Figure 3 [19].

The critical section is again considered to be the root of the rectangular wingbox, which corresponds to element 4 in the model (Figure 2). To calculate the static stress, the normal stress due to bending (σ_b) and shear stress due to torsion (τ) at the critical section are first obtained from the out-of-plane curvature and twist of the fourth element of the model, *i.e.*,

$$\sigma_b = E\tfrac{h}{2}\,\kappa_{oop}|_{\text{wing root}} \tag{9}$$

$$\tau = \frac{GJ}{2wht_w}\,\theta'|_{\text{wing root}}, \tag{10}$$

where the $\theta'|_{\text{wing root}}$ is the twist rate of the beam evaluated at the critical section and the torsion constant J is obtained using Bredt's equation:

$$\frac{1}{J} = \frac{1}{2(wh)^2}\left(\frac{h}{t_h} + \frac{w}{t_w}\right) \tag{11}$$

The bending and torsional stresses are then combined using the von Mises stress relation:

$$\sigma_{2.5\,\text{g}} = \sqrt{\sigma_b^2 + 3\tau^2}. \tag{12}$$

Note that the shear stress here is purely from the wing twist and does not account for the shear stress due to the flexural problem.

2.6 Peak stress constraint

To constrain the peak stress to which the wingbox is subjected, Hoblit's design envelope criterion is used to calculate the peak gust stress σ_{gust} [14], *i.e.*,

$$\sigma_{\text{gust}} = \frac{\text{rms}(\sigma_g)}{\text{rms}(w_G)}\eta_d\,\text{rms}(w_G) = \bar{A}U_{\text{gust}}, \tag{13}$$

where η_d is a peak-to-rms ratio, $\bar{A}$ is the rms value of the stress PSD when the system is excited by a normalized gust signal, and $U_g = \eta_d\,\text{rms}(w)$ is the design gust velocity, obtained from the design requirements.

The total stress is calculate by summing the 2.5-g maneuver stress to the peak gust stress, in order to calculate the margin of safety (MS), given by

$$\text{MS} = \frac{\sigma_{\text{allowable}}}{|\sigma_{\text{gust}} + \sigma_{\text{2.5-g}}|} - 1, \tag{14}$$

where $\sigma_{\text{allowable}}$ is the allowable stress for the application (includes a factor of safety on the corresponding material property).. The margin of safety of the peak gust stress is constrained to be non-negative, *i.e.*,

$$\text{MS} \geq 0. \tag{15}$$

2.7 Fatigue constraint

When formulating an MDO problem that involves gust loads, it is important to incorporate a fatigue constraint to correctly evaluate designs with large stress power at high frequency bands. Even if the peak stress to which these designs are exposed is safe, they may be subjected to a high number of stress cycles that will lead to fatigue damage.

The most widely used method to calculate fatigue damage is to use the Palmgreen-Miner rule combined with the rainflow count of cycles in the stress time history to calculate the damage experienced by the material over time. Since the approach herein is done in the frequency domain, it would be very costly to generate a representative time signal of the stress (*e.g.*, by designing a filter driven by white noise). Instead, the preferred approach is to use Dirklik's empirical method for approximating the rate of damage due to gust [20], and then constraining this damage rate by a limit based on the expected flight hours in turbulence for the lifetime of the airframe. Dirklik's method has been shown to provide good agreement with the time-domain rainflow counting analysis [21].

Dirklik's method for estimating the mean damage rate of the rainflow count of the stress, $\dot{D}^{DK}_{RFC}$, requires the moments λ_0, λ_1, λ_2, λ_4 of the stress PSD, where

$$\lambda_m = \int_0^\infty \omega^m \Phi(\omega)\, \mathrm{d}\omega, \quad m = 0, 1, 2, 3, 4. \tag{16}$$

It is described by:

$$\dot{D}^{DK}_{RFC} = \frac{\nu_p}{C}\sqrt{\lambda_0}\left[D_1 Q^k \Gamma(1+k) + 2^{k/2}\Gamma(1+k/2)(D_2|R|^k + D_3)\right], \tag{17}$$

where:

$$\begin{aligned}
\nu_0 &= \frac{1}{2\pi}\sqrt{\frac{\lambda_2}{\lambda_0}}, & \nu_p &= \frac{1}{2\pi}\sqrt{\frac{\lambda_4}{\lambda_2}}, & \alpha_2 &= \frac{\lambda_2}{\sqrt{\lambda_0\lambda_4}}, \\
x_m &= \frac{\lambda_1}{\lambda_0}\sqrt{\frac{\lambda_2}{\lambda_4}}, & D_1 &= \frac{2(x_m - \alpha_2^2)}{1+\alpha_2^2}, & D_2 &= \frac{1-\alpha_2-D_1+D_1^2}{1-R}, \\
D_3 &= 1 - D_1 - D_2, & Q &= \frac{1.25(\alpha_2 - D_3 - D_2 R)}{D_1}, & R &= \frac{\alpha_2 - x_m - D_1^2}{1-\alpha_2-x_m-D_1+D_1^2},
\end{aligned} \tag{18}$$

The parameters ν_0 and ν_p correspond to the frequency of zero crossing and frequency of peaks of the random signal, respectively, $\Gamma(\cdot)$ is the Gamma function, and C and k are the parameters of the material's S-N curve expressed as $N = C\sigma^{-k}$, which can be obtained from, for example, MIL-HDBK-5J with unity stress ratio.

The expected life in fatigue is then given by

$$\mathbb{E}[\text{fatigue life}] = \frac{1}{\dot{D}_{RFC}^{DK}}. \tag{19}$$

A safety factor of 3 is usually applied to this value, and an additional factor of 1.5 is applied to allow for the variability of loading between different aircraft of the same type [22]. The appropriate gust instensity for using with the von Kàrmàn model when doing the fatigue life calculation described can be obtained from, *e.g.*, MIL-HDBK-1797.

2.8 Trim

The optimization problem needs an additional constraint in order to enforce the trim condition. The condition enforced in this problem is that the net vertical force is equal to zero ($F_z = 0$). The trim angle of attack is considered as a design variable and solved for.

2.9 MDO problem formulation

In order to illustrate the integration of the proposed combination of sensitivity function parameterization, gust load constraint (both peak and fatigue), and Bode integral constraint, a wingbox optimization problem is defined as given in Table 1.

Table 1: Optimization problem.

minimize	$4b\rho(t_d d + t_w w)$	(wing mass)
with respect to	$t_w, t_d,$	(structural design variables)
	α	(trim design variable)
	$\omega_c, \omega_0, g_0, q,$	(sensitivity function design variables)
subject to	$\text{MS} = \dfrac{\sigma_{\text{allowable}}}{\lvert\sigma_{\text{gust}} + \sigma_{\text{2.5-g}}\rvert} - 1 \geq 0$	(peak gust stress constraint)
	$\log(\mathbb{E}[\text{fatigue life}]) \geq \log(\text{FS} \cdot \text{design life})$	(fatigue constraint)
	$F_z = 0$	(trim constraint)
	$\displaystyle\int_0^{\omega_b} \log\lvert S(j\omega)\rvert \, \mathrm{d}\omega = \pi \sum_{k=1}^{n_u} \mathrm{Re}(\lambda_k)$	(Bode integral relation constraint)

The thickness of the sides of the symmetrical rectangular wingbox cross-section are used as the structural design variables, while the parameters of the sensitivity function are used as control design variables. Additionally the angle of attack is also included as a design variable to provide the necessary degree of freedom allow the trim condition to be satisfied. A schematic drawing of the wingbox cross section is shown in Figure 3. This cross section is used to calculate the stiffness and mass properties that are fed into UM/NAST.

This MDO problem was implemented in the OpenMDAO optimization framework [23] and it uses UM/NAST for calculating the constraints. It is solved using SciPy's SLSQP optimizer and the gradients are obtained using finite differences, for simplicity.

3 OPTIMIZATION RESULTS

The MDO problem defined in Table 1 is solved with the problem parameters chosen as described in Table 2 considering both the expansion of the design space with control-related design variables (closed-loop design) and the unitary sensitivity function case (open-loop design). The resulting optimum values for the design variables and response functions are shown in Table 3.

Table 2: Optimization parameters.

Parameter	Value	Source
Available bandwidth	30 Hz	Assumed technological level
Flight speed	120 m/s	Design requirements
Flight Altitude	20000 ft	
Turbulence scale	2500 ft	Typical choice for altitude
Fatigue gust intensity	10 ft/s	MIL-STD-1797A
Peak gust intensity	70 ft/s	Hoblit [14]
Young's modulus	70 GPa	Aluminum 7075-T6
Density	2700 kg/m^3	
Shear modulus	26 GPa	
Yield strength	430 MPa	
$\sigma_{\text{allowable}}$	287 MPa	
k	5.80	MIL-HDBK-5J p. 3-409 Fig. 3.7.6.1(d)
$\log_{10} C$	14.86 $\sqrt[k]{\text{ksi}}$	

From Table 3, the closed-loop design shows a decrease of 22% in the thickness of the upper and lower sections of the wingbox (t_w), while keeping the sides relatively unchanged ($\Delta t_h = -0.5\%$). This caused a reduction of 21% on the wingbox weight, while satisfying the fatigue constraint, which is active for both designs. The closed-loop design saw a decrease in the peak gust stress of 3%.

Figure 4 shows the frequency response and power spectral distributions (PSDs) of gust speed and stress of the optimal designs. It also illustrates Equation (2). The inputs for the calculation are the von Kàrmàn gust PSD (Figure 4a) and the gust speed to stress frequency response (Figure 4b). Multiplying them together results in the open-loop stress PSD (Figure 4c), which is used to calculate the expected fatigue life and the peak gust margin of safety for the open-loop design. The optimized shape of the sensitivity function for the closed-loop design is shown in Figure 4d, in logarithmic form. Since the plant is open-loop stable, Bode's integral relation states that it should integrate to zero. Applying this sensitivity function to the open-loop gust stress PSD results in the closed-loop gust stress PSD (Figure 4e). This curve is used to calculate the fatigue and peak gust constraints for the closed-loop design. The three peaks observed in the gust to stress frequency response correspond to the short-period, and first and second out-of-plane bending modes respectively.

The optimal sensitivity function provides attenuation of the response for the modes below its crossover frequency of 5.7 Hz, which corresponds to the two most prominent peaks in the

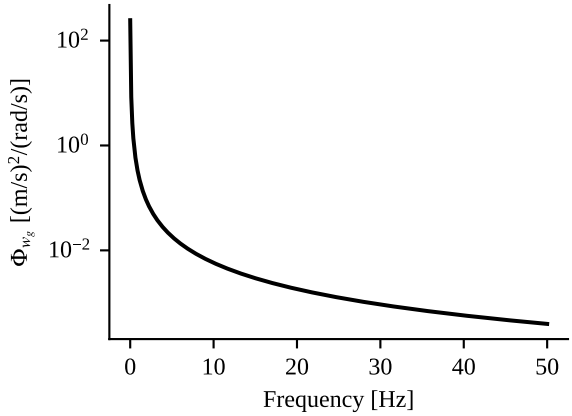

(a) Von Kàrmàn gust power spectral density

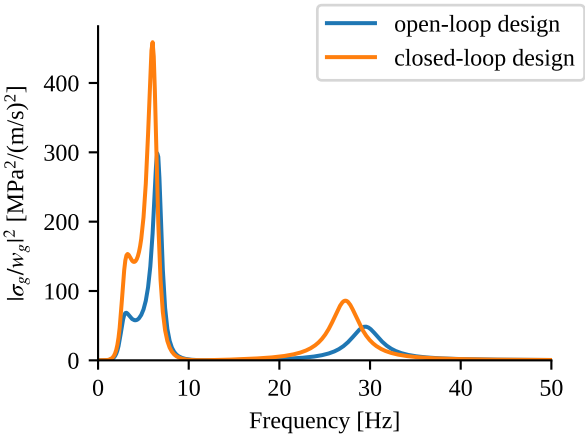

(b) Gust velocity to stress frequency response

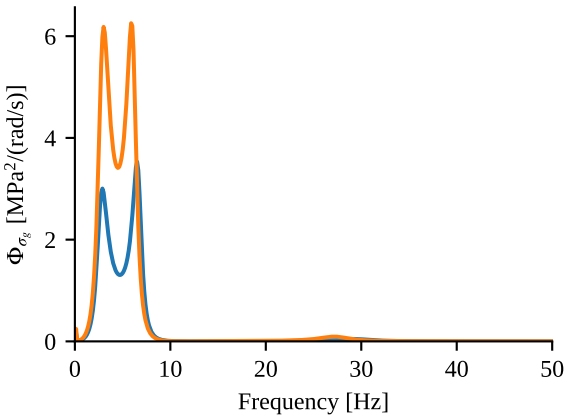

(c) Open-loop gust stress power spectral density

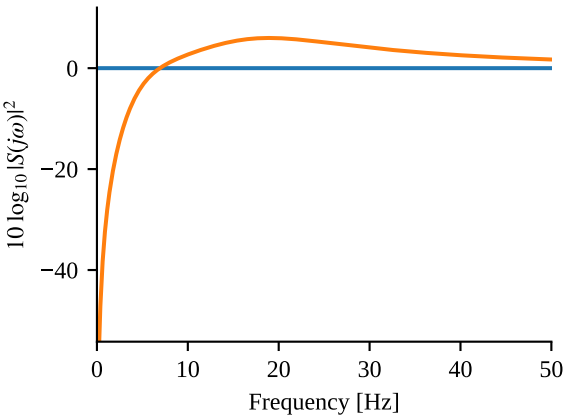

(d) Sensitivity function

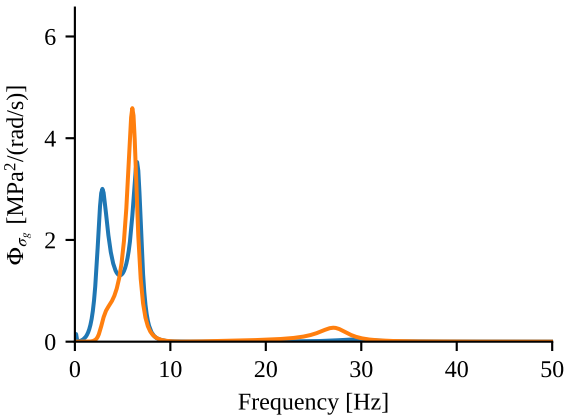

(e) Closed-loop gust stress power spectral density

Figure 4: Power spectral distributions and transfer functions of optimal designs.

Table 3: Optimization results.

(a) Design variables

	Open-loop design	Closed-loop design	Δ [%]	Lower bound	Upper bound
t_h [mm]	0.84	0.83	-0.5%	0.1	10
t_w [mm]	2.27	1.77	-22.2%	0.1	10
α [deg]	2.52	2.49	-1.1%	-10	10
g_0	-	2	-	1	2
q_0	-	1	-	1	10
ω_0 [Hz]	-	18.84	-	10	20
ω_c [Hz]	-	5.70	-	0	10

(b) Response variables

	Open-loop design	Closed-loop design	Δ [%]	Lower bound	Upper bound
$\log_{10}\mathbb{E}$[fatigue life in hours]	5.00	5.00	0.0%	5	-
peak stress due to gust [GPa]	0.26	0.25	-3.2%	-	-
peak stress margin of safety	0.10	0.13	-	0	-
wingbox weight [kg/m]	3.56	2.81	-21.0%	-	-

stress PSD. The first peak is entirely suppressed, while the second peak is attenuated but still rises higher than the corresponding peak from the open-loop design. The sensitivity function assumes values larger than one in the 10–30 Hz range, which corresponds to an increase in the gust stress distribution in this frequency range, which has a peak around 28 Hz. The net effect is that the spectral content of the gust stress is shifted to higher frequencies, but has its RMS value reduced. This causes a reduction in the peak gust stress, reflected in the higher margin of safety for this metric, while the expected life in fatigue calculated by the Dirklik's method remains unchanged.

The fact that the margin of safety for the peak gust stress increased while the fatigue life remained constant highlights that, while the fatigue constraint is important for sizing the open-loop design, it is even more so when designing for closed-loop. Due to the inherit limitations in bandwidth of any control system, they tend to be more effective at decreasing loads at lower frequencies, which in turn leads to optimal designs with increased loads at higher frequencies.

The optimal closed-loop design is sensitive to choices in the parameterization of the sensitivity function and to the value chosen for the available bandwidth ω_b. Together, these parameters reflect the assumed technological level for the control system, its sensors and actuators.

4 CONCLUDING REMARKS

This paper introduced a method for integrating gust load alleviation considerations in the multidisciplinary design optimization process. The new approach is controller-agnostic, that is, it does not requires *a priori* definition of the control architecture or the the co-design of the controller gains during the airframe sizing. However, it does bring control considerations up front so to guarantee the existence of a controller that will satisfy the expected load alleviation. This paper also showcased newly developed features to integrate the free-flying vehicle modeling

framework (UM/NAST) in the general-purpose OpenMDAO framework and its use in aircraft design.

The effect of gust loads and GLA in the design is assessed through two metrics: peak stress and expected fatigue life. Both are evaluated in the frequency domain, based on the power spectral density of the stress induced by gust. These metrics can be used for open-loop designs as well as for closed-loop designs by incorporating the effect of the controller through a parameterized sensitivity function. These parameters are included in the problem as design variables, and the Bode integral relation is enforced as a constraint. The choice of parameter value ranges to be used by the sensitivity function is connected to the technological level of the implied controller.

The proposed approach of parameterizing the sensitivity function was able to capture the load reducing behaviour of a GLA controller, while satisfying the Bode integral relation within the available actuation bandwidth, and without directly designing such controller. The MDO design including consideration of GLA control showed significant weight reduction if compared to the optimal design without control considerations, while still satisfying constraints on fatigue life and peak stress due to gust.

For future work aiming to increase the representativeness of the design problem, more points in the flight envelope must be considered. Also, additional constraints for flying with a failed GLA system should be imposed.

5 ACKNOWLEDGEMENTS

The material of this paper is based upon work supported by Airbus in the frame of the Airbus-Michigan Center for Aero-Servo-Elasticity of Very Flexible Aircraft.

6 REFERENCES

[1] Suzuki, S. and Yonezawa, S. (1993). Simultaneous structure/control design optimization of a wing structure with a gust load alleviation system. *Journal of aircraft*, 30(2), 268–274.

[2] Hunten, K., Zink, S., Flansburg, B., et al. (2007). A systems mdo approach for an unmanned aerial vehicle. In *48th AIAA/ASME/ASCE/AHS/ASC Structures, Structural Dynamics, and Materials Conference*. American Institute of Aeronautics and Astronautics. ISBN 978-1-62410-013-0. doi:10.2514/6.2007-1877.

[3] Haghighat, S., Martins, J. R. R. A., and Liu, H. H. T. (2012). Aeroservoelastic design optimization of a flexible wing. *Journal of Aircraft*, 49, 432–443. ISSN 0021-8669. doi:10.2514/1.C031344.

[4] Xu, J. and Kroo, I. (2014). Aircraft design with active load alleviation and natural laminar flow. *Journal of Aircraft*, 51(5), 1532–1545. doi:10.2514/1.c032402.

[5] Stanford, B. (2020). Optimal aircraft control surface layouts for maneuver and gust load alleviation. In *AIAA Scitech 2020 Forum*. pp. 1–10.

[6] Vartio, E., Shaw, E., and Vetter, T. (2008). Gust load alleviation flight control system design for a sensorcraft vehicle. In *26th AIAA Applied Aerodynamics Conference*. American Institute of Aeronautics and Astronautics. ISBN 978-1-60086-987-7. doi:10.2514/6.2008-7192.

[7] Zeng, J., Moulin, B., de Callafon, R., et al. (2010). Adaptive feedforward control for gust load alleviation. *Journal of Guidance, Control, and Dynamics*, 33. ISSN 0731-5090. doi:10.2514/1.46091.

[8] Dillsaver, M., Cesnik, C., and Kolmanovsky, I. (2011). Gust load alleviation control for very flexible aircraft. In *AIAA Atmospheric Flight Mechanics Conference*. American Institute of Aeronautics and Astronautics. ISBN 978-1-62410-153-3. doi:10.2514/6.2011-6368.

[9] Haghighat, S., Liu, H. H. T., and Martins, J. R. R. A. (2012). Model-predictive gust load alleviation controller for a highly flexible aircraft. *Journal of Guidance, Control, and Dynamics*, 35. ISSN 0731-5090. doi:10.2514/1.57013.

[10] Ting, K.-Y., Mesbahi, M., Livne, E., et al. (2022). Wind tunnel study of preview H_2 and H_∞ control for gust load alleviation for flexible aircraft. In *AIAA Scitech 2022 Forum*. American Institute of Aeronautics and Astronautics. ISBN 978-1-62410-631-6. doi:10.2514/6.2022-2489.

[11] Díaz, J. M., Costa-Castelló, R., and Dormido, S. (2019). Closed-loop shaping linear control system design: An interactive teaching/learning approach [focus on education]. *IEEE Control Systems*, 40. ISSN 1941000X. doi:10.1109/MCS.2019.2925255.

[12] Li, Y. and Lee, E. (1993). Stability robustness characterization and related issues for control systems design. *Automatica*, 29(2), 479 – 484. ISSN 0005-1098. doi:https://doi.org/10.1016/0005-1098(93)90142-G.

[13] Stein, G. (2003). Respect the unstable. *IEEE Control Systems Magazine*, 23(4), 12–25. doi:10.1109/MCS.2003.1213600.

[14] Hoblit, F. M. (1988). *Gust Loads on Aircraft: Concepts and Applications*. Reston, Virginia: American Institute of Aeronautics and Astronautics.

[15] Skogestad, S. and Postlethwaite, I. (2007). *Multivariable feedback control: analysis and design*. John Wiley & Sons, Ltd, 2 ed.

[16] Su, W. and Cesnik, C. E. S. (2010). Nonlinear aeroelasticity of a very flexible blended-wing-body aircraft. *Journal of Aircraft*, 47(5), 1539–1553. doi:10.2514/1.47317.

[17] Sagebaum, M., Albring, T., and Gauger, N. R. (2019). High-performance derivative computations using codipack. *ACM Transactions on Mathematical Software (TOMS)*, 45(4). doi:10.1145/3356900.

[18] Laub, A. (1981). Efficient multivariable frequency response computations. *IEEE Transactions on Automatic Control*, 26(2), 407–408.

[19] Cesnik, C. E. S. and Hodges, D. H. (1997). Vabs: A new concept for composite rotor blade cross-sectional modeling. *Journal of the American Helicopter Society*, 42(1), 27–38.

[20] Dirlik, T. (1985). *Application of computers in fatigue analysis*. Ph.D. thesis, University of Warwick.

[21] Benasciutti, D. and Tovo, R. (2006). Comparison of spectral methods for fatigue analysis of broad-band gaussian random processes. *Probabilistic Engineering Mechanics*, 21(4), 287–299.

[22] Megson, T. H. G. (2016). *Aircraft structures for engineering students*. Butterworth-Heinemann.

[23] Gray, J. S., Hwang, J. T., Martins, J. R. R. A., et al. (2019). OpenMDAO: An Open-Source Framework for Multidisciplinary Design, Analysis, and Optimization. *Structural and Multidisciplinary Optimization*, 59, 1075–1104. doi:10.1007/s00158-019-02211-z.

COPYRIGHT STATEMENT